



Article

Virtual Screening Strategy and In Vitro Tests to Identify New Inhibitors of the Immunoproteasome

Giulia Culetta ^{1,2} , Marco Tutone ^{1,*} , Roberta Ettari ² , Ugo Perricone ³ , Carla Di Chio ²,
Anna Maria Almerico ¹ and Maria Zappalà ²

¹ Dipartimento di Scienze e Tecnologie Biologiche Chimiche e Farmaceutiche (STEBICEF),
Università degli Studi di Palermo, Via Archirafi 32, 90123 Palermo, Italy

² Dipartimento di Scienze Chimiche, Biologiche, Farmaceutiche ed Ambientali, Università di Messina, Viale
Annunziata, 98168 Messina, Italy

³ Drug Discovery Unit, Fondazione Ri.MED, 90133 Palermo, Italy

* Correspondence: marco.tutone@unipa.it

Abstract: Immunoproteasome inhibition is a promising strategy for the treatment of hematological malignancies, autoimmune diseases, and inflammatory diseases. The design of non-covalent inhibitors of the immunoproteasome $\beta 1i/\beta 5i$ catalytic subunits could be a novel approach to avoid the drawbacks of the known covalent inhibitors, such as toxicity due to off-target binding. In this work, we report the biological evaluation of thirty-four compounds selected from a commercially available collection. These hit compounds are the outcomes of a virtual screening strategy including a dynamic pharmacophore modeling approach onto the $\beta 1i$ subunit and a pharmacophore/docking approach onto the $\beta 5i$ subunit. The computational studies were first followed by in vitro enzymatic assays at 100 μM . Only compounds capable of inhibiting the enzymatic activity by more than 50% were characterized in detail using Tian continuous assays, determining the dissociation constant (K_i) of the non-covalent complex where K_i is also the measure of the binding affinity. Seven out of thirty-four hits showed to inhibit $\beta 1i$ and/or $\beta 5i$ subunit. Compound 3 is the most active on the $\beta 1i$ subunit with $K_i = 11.84 \pm 1.63 \mu\text{M}$, and compound 17 showed $K_i = 12.50 \pm 0.77 \mu\text{M}$ on the $\beta 5i$ subunit. Compound 2 showed inhibitory activity on both subunits ($K_i = 12.53 \pm 0.18$ and $K_i = 31.95 \pm 0.81$ on the $\beta 1i$ subunit and $\beta 5i$ subunit, respectively). The induced fit docking analysis revealed interactions with Thr1 and Phe31 of $\beta 1i$ subunit and that represent new key residues as reported in our previous work. Onto $\beta 5i$ subunit, it interacts with the key residues Thr1, Thr21, and Tyr169. This last hit compound identified represents an interesting starting point for further optimization of $\beta 1i/\beta 5i$ dual inhibitors of the immunoproteasome.

Keywords: immunoproteasome; $\beta 1i$ subunit; $\beta 5i$ subunit; docking; induced fit docking; pharmacophore modeling; in vitro enzymatic assay



Citation: Culetta, G.; Tutone, M.; Ettari, R.; Perricone, U.; Di Chio, C.; Almerico, A.M.; Zappalà, M. Virtual Screening Strategy and In Vitro Tests to Identify New Inhibitors of the Immunoproteasome. *Int. J. Mol. Sci.* **2023**, *24*, 10504. <https://doi.org/10.3390/ijms241310504>

Academic Editors: Robert P. Ostrowski and Masahiro Fujimuro

Received: 26 April 2023

Revised: 16 June 2023

Accepted: 20 June 2023

Published: 22 June 2023



Copyright: © 2023 by the authors. Licensee MDPI, Basel, Switzerland. This article is an open access article distributed under the terms and conditions of the Creative Commons Attribution (CC BY) license (<https://creativecommons.org/licenses/by/4.0/>).

1. Introduction

The ubiquitin–proteasome system (UPS) is the main non-lysosomal proteolytic system involved in the intracellular protein turnover in eukaryotic cells [1]. In normal cells, the proteasome proteolytic activity is responsible for regular cell cycle progression, homeostasis control, and immune surveillance [2,3]. Defects and aberrations in UPS can lead to uncontrolled cell proliferation and tumor development. For these reasons, novel approaches to cancer therapy exist based on proteasome inhibition [1,4,5].

The 20S constitutive proteasome is composed of four stacked rings: the two inner β -rings, which contain the catalytic subunit, and two outer α -rings, whose function is structural [6].

The catalytic subunits $\beta 1c$, $\beta 2c$, and $\beta 5c$ are responsible for the caspase-like (C-L), trypsin-like (T-L), and chymotrypsin-like (ChT-L) activities of the proteasome, respectively,

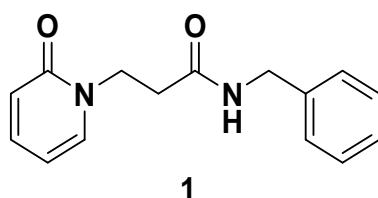
with the ChT-L activity being currently considered the primary target for the development of novel anticancer agents [7].

In addition to the constitutive proteasome, vertebrates possess a specialized form of the proteasome, known as immunoproteasome, expressed in monocytes and lymphocytes and responsible for cell-mediated immunity and for the generation of major histocompatibility complex (MHC) class I ligands [8,9]. Under the stimuli of IFN- γ and TNF- α , the β c core particles are replaced by β 1i, β 2i, and β 5i subunits. While β 2i and β 5i perform the same type of activities of the β 2c and β 5c subunits, differently, the replacement of β 1c with β 1i brings the caspase-like activity to background levels. Prominent levels of immunoproteasome core particles have been detected in many autoimmune diseases, such as rheumatoid arthritis and systemic lupus erythematosus, and in a panel of inflammatory diseases, such as Crohn's disease, inflammatory bowel disease, and ulcerative diseases. At the same time, overexpression of immunoproteasome core particles has been detected in hematological malignancies, such as multiple myeloma [9].

In this context, several β 5i and/or β 1i immunoproteasome-selective inhibitors have been identified [10–12]. Recently, particular attention has been devoted to the development of noncovalent proteasome inhibitors, which are free from side effects related to irreversible inhibition of a human target [13–16].

In this research area, our research group has been actively involved in the development of novel 20S proteasome inhibitors [17–22]. More recently, considering the variety of therapeutic applications of the development of immunoproteasome-selective inhibitors, we developed novel noncovalent immunoproteasome inhibitors.

Among all the synthesized immunoproteasome inhibitors, we identified a panel of active inhibitors with K_i values in the low micromolar or sub-micromolar ranges towards the β 5i and/or β 1i subunits of immunoproteasome [23]. Compound 1, *N*-benzyl-2-(2-oxopyridin-1(2*H*)-yl)propanamide (Scheme 1), was shown to be the most potent and selective inhibitor with a K_i value of 21 nM against the sole β 1i subunit.



Scheme 1. Structure of the selective β 1i inhibitor 1.

The mechanism of the non-covalent inhibition of this compound has been investigated using advanced molecular dynamics methods such as MD-binding (MDB) and Binding Pose MetaDynamics (BPMD). Moreover, an advanced docking method, Induced Fit Docking (IFD), was used for further investigation [24]. These approaches allowed for analyzing the binding mechanism, gaining insights into the ligand entrance pathway, and elucidating the dynamic behavior of the ligand within the binding cavity, providing a dynamic point of view for the definition of the pharmacophore features.

In this study, we employed these collected outcomes to obtain a dynamic pharmacophore model for β 1i inhibitors. Additionally, to find new inhibitors of the β 5i subunit, we developed a structure-based study using docking and pharmacophore models approaches, starting from the β 5i subunit co-crystallized with PR-957 inhibitor (PDB ID: 3UNF).

Both pharmacophore models were used for a virtual screening campaign on commercially available compound collection of 2 million compounds (hereby called compound library) that allowed the selection of thirty-four potential inhibitors from three commercial databases for inhibition assays against β 1i/ β 5i subunits.

2. Results and Discussion

2.1. β 1i Pharmacophore Modeling

The previous MD study [24] allowed identifying three representative poses (pose 1, pose 2, and pose 3) that elucidated the dynamic behavior and stability of compound 1 within the binding cavity. The interactions pattern of inhibition included two H-bonds between the amide group and Ser21 and Gly47, a π -stacking between the benzyl group and Phe31, and a cation- π stacking interaction between the 2-pyridone moiety and the epsilon amino group of Lys33. These pose models were used to carry out a pharmacophore approach for the β 1i subunit.

For each pose, pharmacophore models were generated using LigandScout [25] PHASE [26]. In LigandScout, pose1 showed three features: a hydrogen bond acceptor (HBA), a hydrogen bond donor (HBD), and a hydrophobic interaction (Figure 1a). Pose2 showed a hydrogen bond acceptor (HBA) and a hydrophobic interaction (Figure 1b). Pose3 was characterized by one hydrogen bond acceptor (HBA), one hydrogen bond donor (HBD), and two hydrophobic interactions (Figure 1c). A merged pharmacophore model [27,28] including all features observed for each pose was constructed and improved by removing the redundant features. The final model is characterized by five features: two hydrogen bond acceptors (HBA), one hydrogen bond donor (HBD), and two hydrophobic interactions (Figure 1d). The model was retrospectively validated using the active and decoy datasets and performing the receiver operating characteristic (ROC) curve analysis. The ROC curves plot the sensitivity (true positive rate-TPR) against the specificity (false positive rate-FPR). The area under the curve (AUC) is used to assess the accuracy of the model. The grey dashed line represents the random line (AUC = 0.5); the blue curve represents the AUC of the model (AUC must be greater than 0.5). The enrichment factor is the number of active compounds found compared to their presence in the entire database. The model built with LigandScout showed values of $AUC_{1\%} = 1$ and $EF_{1\%} = 15.3$ (Figure 2a).

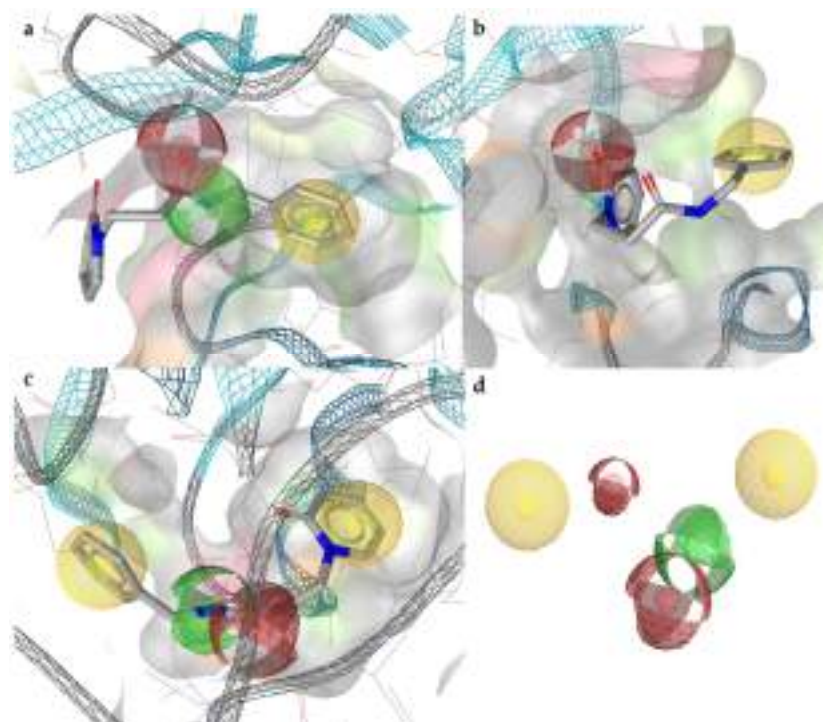


Figure 1. LigandScout pharmacophore model of (a) Pose1, (b) Pose2, (c) Pose3, and (d) Merged. Aromatic interactions are represented in yellow spheres, hydrogen bond donors in green spheres, and hydrogen bond acceptors in red spheres.

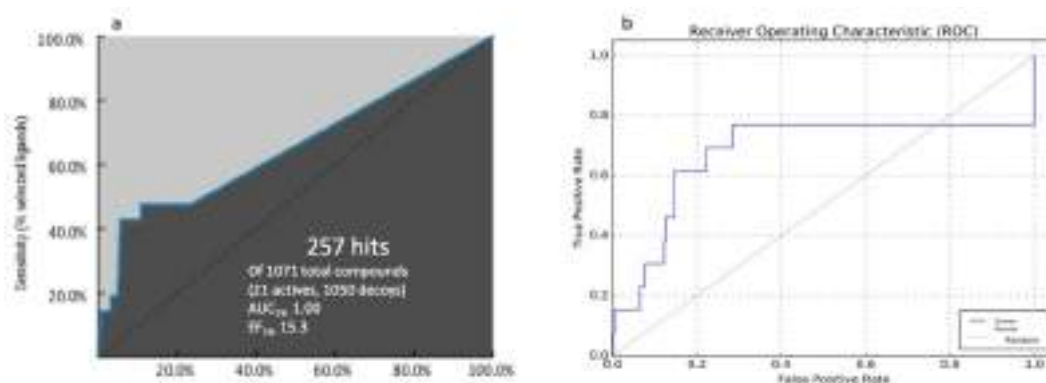


Figure 2. ROC curves of (a) LigandScout model and (b) PHASE model for $\beta 1i$ subunit.

The same procedure was carried out with PHASE. Pose1 showed three features: two hydrogen bond acceptors, one hydrogen bond donor, and two aromatic rings (Figure 3a). In Pose2, one aromatic ring was recovered (Figure 3b). Pose3 was characterized by one hydrogen bond acceptor, one hydrogen bond donor, and one aromatic ring (Figure 3c).

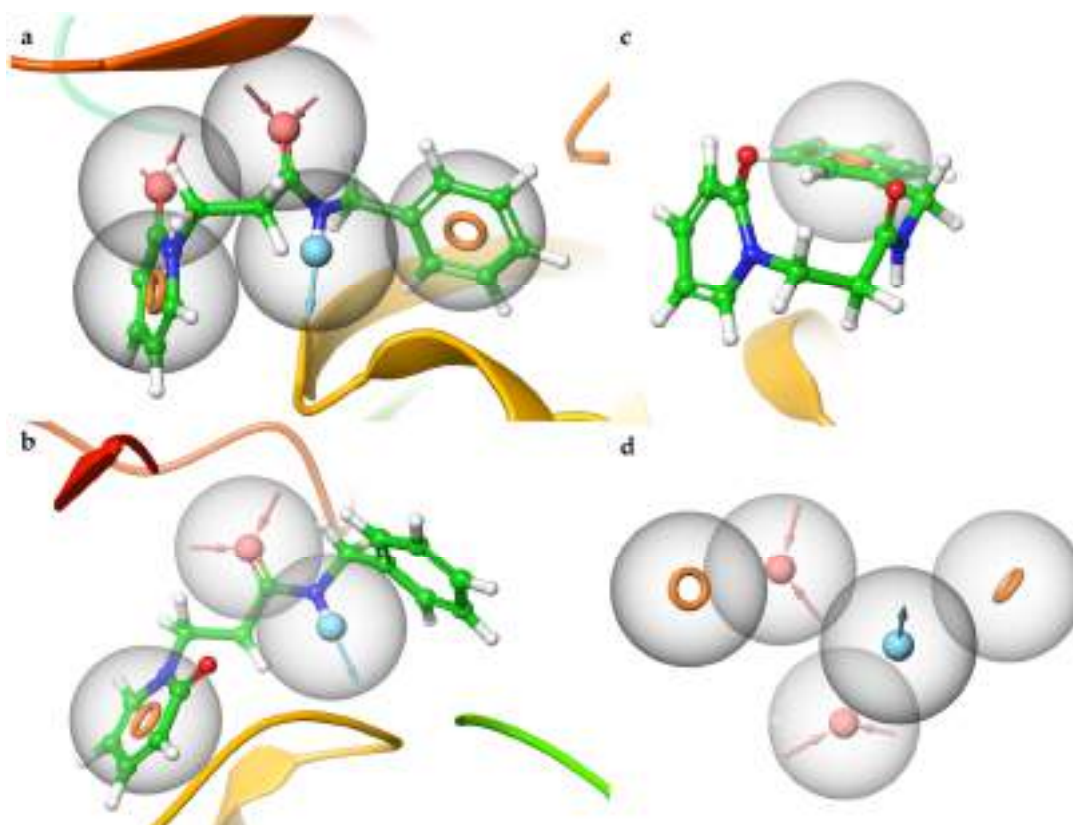


Figure 3. PHASE pharmacophore models of (a) Pose1, (b) Pose2, (c) Pose3, and (d) Merged. The aromatic rings are represented in orange rings, hydrogen bond donors in blue spheres, and hydrogen bond acceptors in pink spheres.

As previously, the PHASE-merged pharmacophore model was then obtained with all features observed in the three poses. Two hydrogen bond acceptors, one hydrogen bond donor, and two aromatic rings (Figure 3d).

This model was also retrospectively validated and showed values of $AUC_{1\%} = 0.60$ and $EF_{1\%} = 4.9$ (Figure 2b).

2.2. $\beta 5i$ Docking and Pharmacophore Modeling

For the $\beta 5i$ subunit, a structure-based study was carried out on the experimental structure of the immunoproteasome (PDB ID: 3UNF). In this experimental structure of immunoproteasome, the $\beta 5i$ subunit is complexed with the PR-957 inhibitor. This ligand was covalently bound to Thr1 of the $\beta 5i$ subunit. The PR-957 inhibitor was structurally modified by breaking the covalent bond and filling in the open valence [29]. The portion of the epoxy ring responsible for the covalent attack on Thr1 was opened (Figure 4a,b).

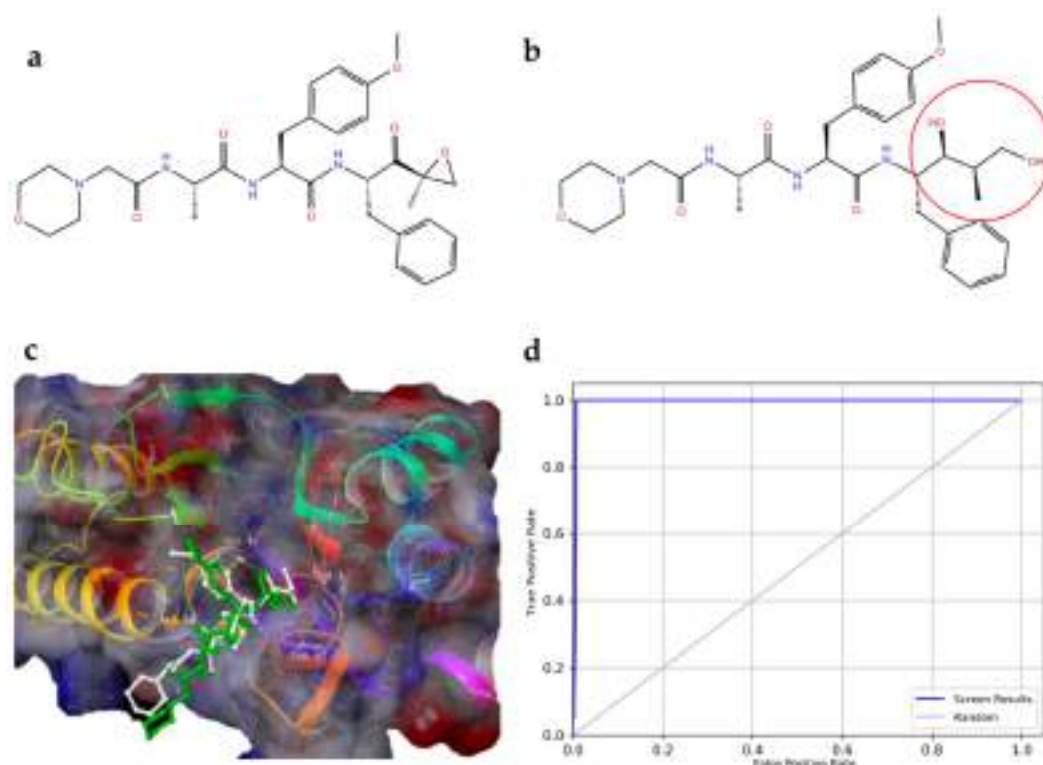


Figure 4. (a) PR-957 covalent epoxyketone; (b) Modified PR-957, free of the epoxy ring portion (circled in red); (c) Superposition of the re-docked poses of PR-957: modified (green) and co-crystallized (white); (d) ROC curve for the retrospective analysis of $\beta 5i$ subunit.

A re-docking protocol was performed using Glide with XP precision to validate the ability to reproduce the experimental position of the co-crystallized ligand. The experimental and docking positions differ only in the epoxy moiety responsible for the covalent interactions. The root means square deviation (RMSD) between the re-docked and crystal conformation of PR-957 was 1.77 Å, less than 2 Å, indicating that Glide XP has a reliable scoring function for this study. The docking protocol was further validated using a $\beta 5i$ validation database of active and decoy compounds. The model showed values of $AUC_{1\%} = 0.90$ and $EF_{1\%} = 27$ (Figure 4c,d).

Moreover, the docking method employed reports more than simple contact scoring by combining structural and energetic information between PR-957 and the active site. The docking post-processing outcomes were used to develop an e-pharmacophore hypothesis. The pharmacophore features with an energetic value < 0.5 kcal/mol were retained and used to compose the pharmacophore hypothesis. The e-pharmacophore hypothesis includes one hydrogen bond acceptor (A7), two hydrogen bond donors (D8 and D11), and two aromatic rings (R17 and R18). The energy values for the favorable features in the hypothesis are A3 -0.63 kcal/mol, D8 -1.60 kcal/mol, D11 -0.70 kcal/mol, R17 -0.52 kcal/mol, and R18 -1.60 kcal/mol (Figure 5a). The higher absolute value of the feature energy indicates that the ligand atom mapping has a higher interaction energy with amino acids. This five-point pharmacophore model was retrospectively validated. It showed $AUC_{1\%} = 0.40$

and $EF_{1\%} = 2$, so we decided to recalculate these values by omitting at least one feature. Figure 5b,c shows the ROC curves for the e-pharmacophore hypothesis with features zero and one omitted. The $AUC_{1\%}$ improved up to 0.84.

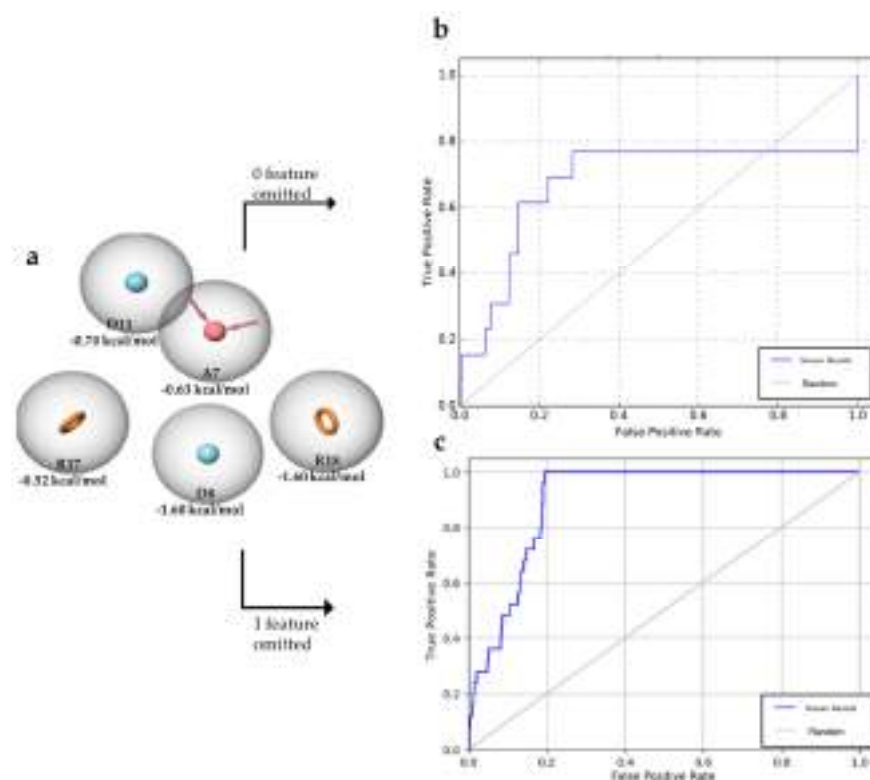


Figure 5. (a) E-pharmacophore hypothesis for $\beta 5i$, five features: two aromatic rings (orange), two hydrogen bond donors (blue), and a hydrogen bond acceptor (red). (b) ROC curves, zero feature omitted and (c) one feature omitted.

LigandScout was also used to build a static pharmacophore starting from the docked position of PR-597. The model was improved by removing redundant features. Then, a six-feature model was obtained: three hydrogen bond donors (HBD), two hydrogen bond acceptors (HBA), and one aromatic interaction (Figure 6a) and a retrospective validation showed $AUC_{1\%} = 0.92$ and $EF_{1\%} = 21.2$ (Figure 6b).

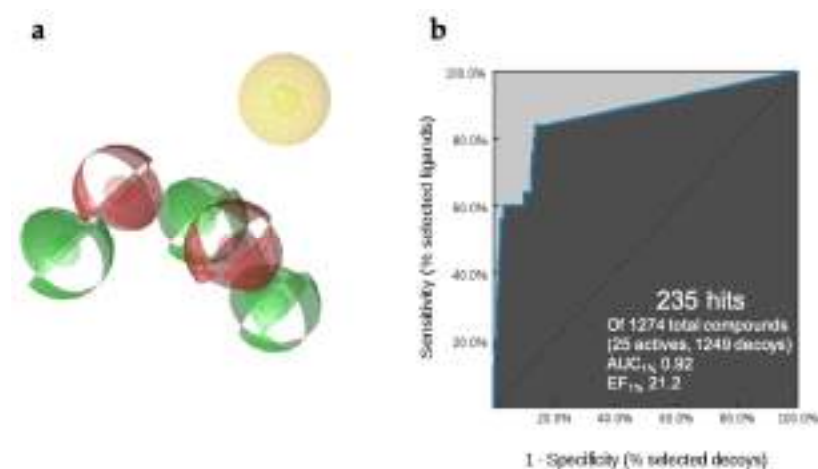


Figure 6. (a) LigandScout model for $\beta 5i$, six features: an aromatic interaction (yellow), three hydrogen bond donors (green), and two hydrogen bond acceptors (red). (b) ROC curve.

2.3. β 1i and β 5i Virtual Screening

The pharmacophore models obtained from the β 1i dynamic studies were used to perform a virtual screening on the compound library (VS β 1i).

The β 5i pharmacophore models were used to perform the virtual screening campaign on the same compound library (VS β 5i) together with a docking analysis. The VS β 5i started with HTVS, SP, and XP docking screening. 1% of the prioritized ligands were retained and then submitted to pharmacophore matching.

The hits obtained from VS β 1i and VS β 5i were ranked according to the consensus score described in the Section 3. The consensus score improved the selection and retrieval of molecules shared between the pharmacophore models for β 1 and β 5. Finally, the hit molecules retrieved after consensus scoring were further evaluated with Induced Fit Docking (IFD) on β 1i and β 5i subunits. IFD confers more flexibility to the protein side chains, allowing the ligands to adjust and optimize binding interactions within the active sites. Visual inspection of the IFD results helped to enrich the final selection. Thirty-four molecules were selected and purchased for in vitro screening against β 1i and β 5i subunits using an enzymatic assay.

These hits were evaluated for their ability to inhibit both subunits of i20S by measuring the rate of hydrolysis of the corresponding fluorogenic substrate Ac-Pro-Ala-Leu-AMC for β 1i and Suc-Leu-Leu-Val-Tyr-AMC for β 5i. MG-132, a reversible inhibitor of the immunoproteasome, was used as a positive control for β 1i and β 5i.

Initially, compounds were screened against each proteolytic subunit at 100 μ M. Only compounds capable of inhibiting the enzymatic activity by more than 50% were characterized in detail using Tian continuous assays. We determined the dissociation constant, i.e., K_i , of the non-covalent complex [E·I], where K_i is also the measure of the binding affinity, since the obtained linear progress curve exhibited a reversible, time-independent inhibition for all the active compounds.

To determine the K_i values (Table 1), seven different concentrations were selected for each compound that passed the initial screening, ranging from those that minimally inhibited to those that completely inhibited the activity of the immunoproteasome subunit.

Table 1. Inhibitory potencies: K_i values (μ M) or percentage of inhibition at 100 μ M of selected compounds on β 1i and β 5i subunits. n.i. is for no inhibition.

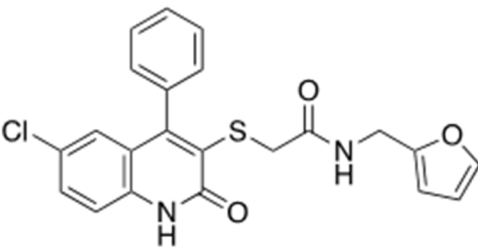
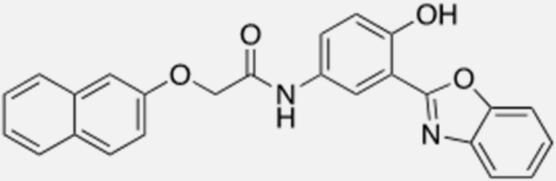
Compound	Structure	β 1i	β 5i
2	 <p>2-((6-chloro-2-oxo-4-phenyl-1,2-dihydroquinolin-3-yl)thio)-N-(furan-2-ylmethyl)acetamide</p>	12.53 \pm 0.18	31.95 \pm 0.81
3	 <p>N-(3-(benzo[d]oxazol-2-yl)-4-hydroxyphenyl)-2-(naphthalen-2-yloxy)acetamide</p>	11.84 \pm 1.63	9%

Table 1. Cont.

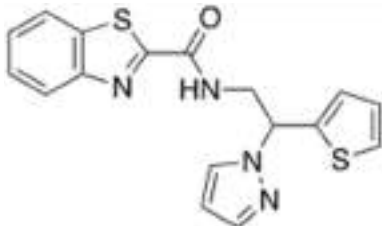
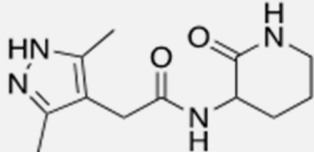
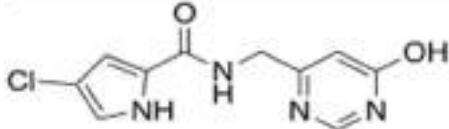
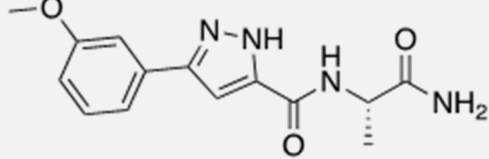
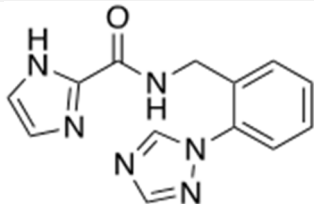
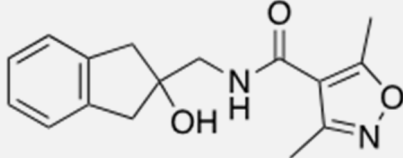
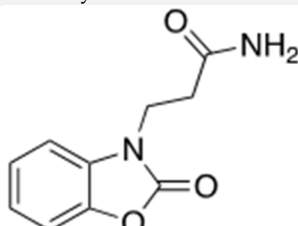
Compound	Structure	β 1i	β 5i
4	 <p><i>N</i>-(2-(1<i>H</i>-pyrazol-1-yl)-2-(thiophen-2-yl)ethyl)benzo[d]thiazole-2-carboxamide</p>	n.i.	23%
5	 <p>2-(3,5-dimethyl-1<i>H</i>-pyrazol-4-yl)-<i>N</i>-(2-oxopiperidin-3-yl)acetamide</p>	n.i.	4%
6	 <p>4-chloro-<i>N</i>-((6-hydroxypyrimidin-4-yl)methyl)-1<i>H</i>-pyrrole-2-carboxamide</p>	n.i.	17%
7	 <p>(<i>S</i>)-<i>N</i>-(1-amino-1-oxopropan-2-yl)-3-(3-methoxyphenyl)-1<i>H</i>-pyrazole-5-carboxamide</p>	n.i.	18%
8	 <p><i>N</i>-(2-(1<i>H</i>-1,2,4-triazol-1-yl)benzyl)-1<i>H</i>-imidazole-2-carboxamide</p>	n.i.	18%
9	 <p><i>N</i>-((2-hydroxy-2,3-dihydro-1<i>H</i>-inden-2-yl)methyl)-3,5-dimethylisoxazole-4-carboxamide</p>	24%	10%
10	 <p>3-(2-oxobenzo[d]oxazol-3(2<i>H</i>)-yl)propanamide</p>	n.i.	28%

Table 1. Cont.

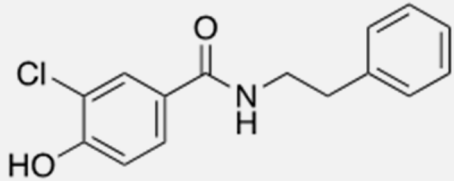
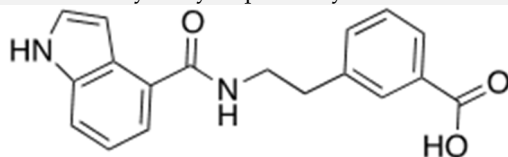
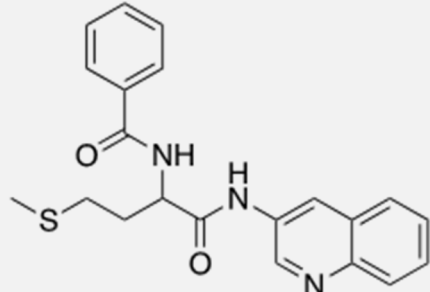
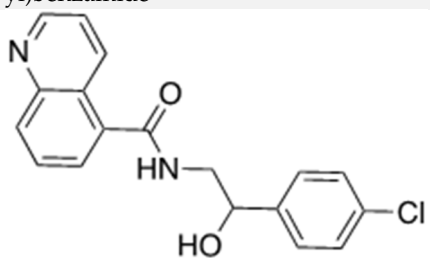
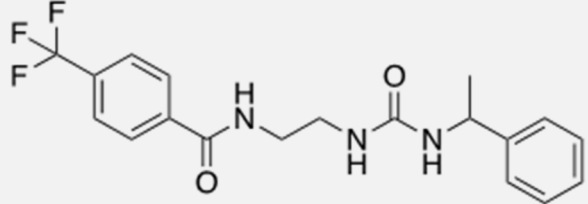
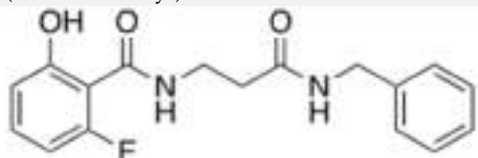
Compound	Structure	β_{1i}	β_{5i}
11	 3-chloro-4-hydroxy-N-phenethylbenzamide	18%	10%
12	 3-(2-(1H-indole-4-carboxamide)ethyl)benzoic acid	2%	23%
13	 <i>N</i> -(4-(methylthio)-1-oxo-1-(quinolin-3-ylamino)butan-2-yl)benzamide	40%	43.68 ± 4.02
14	 <i>N</i> -(2-(4-chlorophenyl)-2-hydroxyethyl)quinoline-5-carboxamide	47%	48.30 ± 4.97
15	 <i>N</i> -(2-(3-(1-phenylethyl)ureido)ethyl)-4-(trifluoromethyl)benzamide	24%	23%
16	 <i>N</i> -(3-(benzylamino)-3-oxopropyl)-2-fluoro-6-hydroxybenzamide	46%	22%

Table 1. Cont.

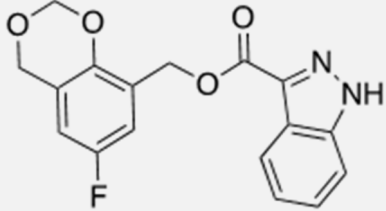
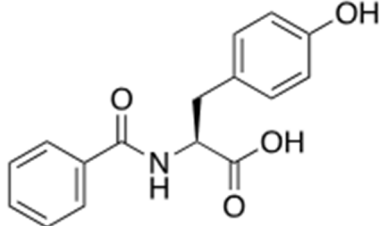
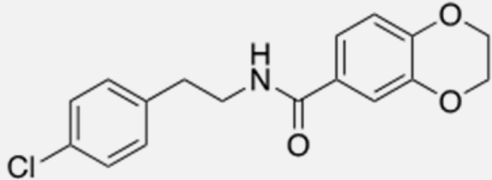
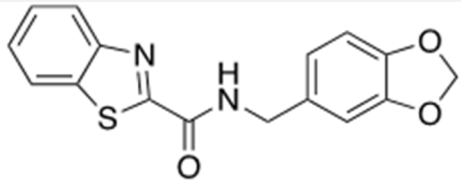
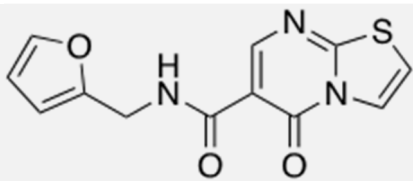
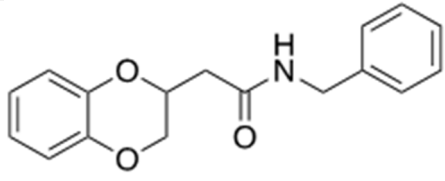
Compound	Structure	β_{1i}	β_{5i}
17	 <p>(6-fluoro-4H-benzo[d][1,3]dioxin-8-yl)methyl 1H-indazole-3-carboxylate</p>	33%	12.50 ± 0.77
18	 <p>(S)-2-benzamido-3-(4-hydroxyphenyl)propanoic acid</p>	15%	1%
19	 <p>N-(4-chlorophenethyl)-2,3-dihydrobenzo[b][1,4]dioxine-6- carboxamide</p>	3%	5%
20	 <p>N-(benzo[d][1,3]dioxol-5-ylmethyl)benzo[d]thiazole-2- carboxamide</p>	25%	36%
21	 <p>N-(furan-2-ylmethyl)-5-oxo-5H-thiazolo[3,2-a]pyrimidine-6- carboxamide</p>	19%	23%
22	 <p>N-benzyl-2-(2,3-dihydrobenzo[b][1,4]dioxin-2-yl)acetamide</p>	31%	32%

Table 1. Cont.

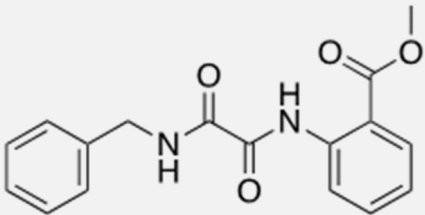
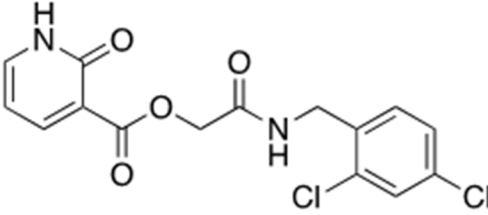
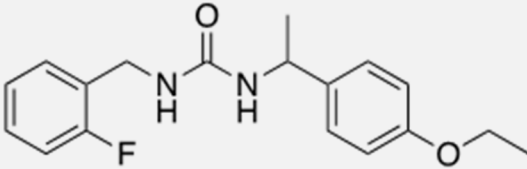
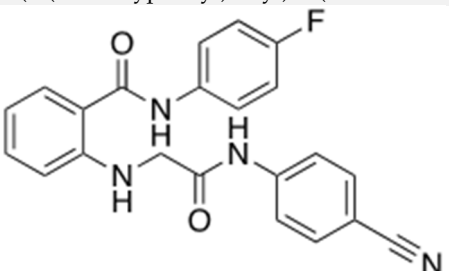
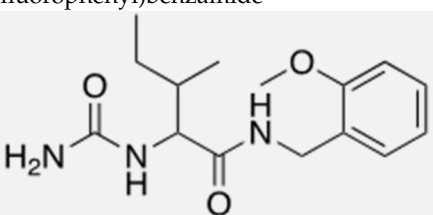
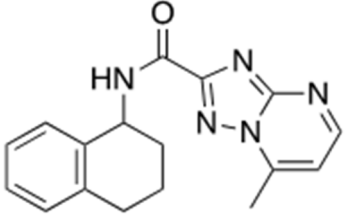
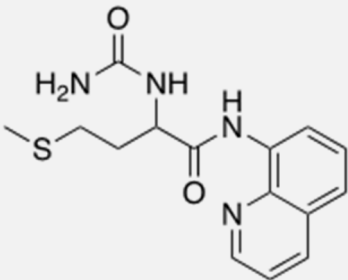
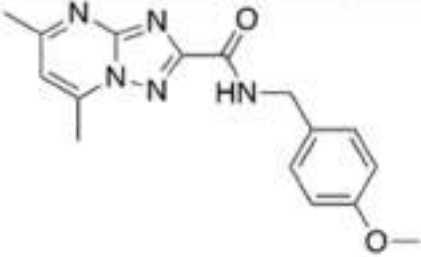
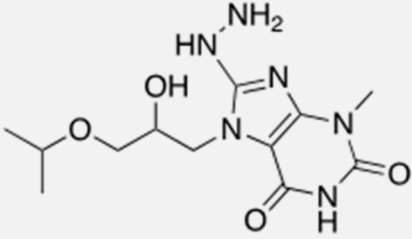
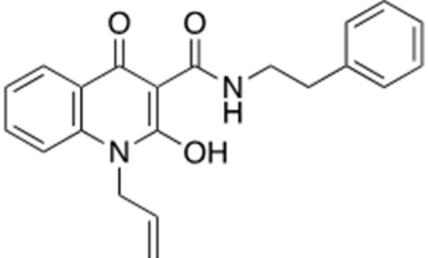
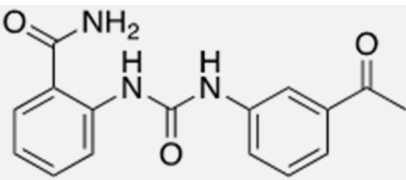
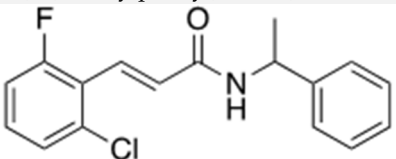
Compound	Structure	β 1i	β 5i
23	 <p>Methyl 2-(2-(benzylamino)-2-oxoacetamido)benzoate</p>	20%	34%
24	 <p>2-((2,4-dichlorobenzyl)amino)-2-oxoethyl 2-oxo-1,2-dihydropyridine-3-carboxylate</p>	21%	34%
25	 <p>1-(1-(4-ethoxyphenyl)ethyl)-3-(2-fluorobenzyl)urea</p>	16%	55%
26	 <p>2-((2-((4-cyanophenyl)amino)-2-oxoethyl)amino)-N-(4-fluorophenyl)benzamide</p>	Fluorescent	Fluorescent
27	 <p>N-(2-methoxybenzyl)-3-methyl-2-ureidopentanamide</p>	27%	23%
28	 <p>7-methyl-N-(1,2,3,4-tetrahydronaphthalen-1-yl)-[1,2,4]triazolo[1,5-a]pyrimidine-2-carboxamide</p>	23%	13%

Table 1. Cont.

Compound	Structure	β_{1i}	β_{5i}
29		45%	47%
	4-(methylthio)-N-(quinolin-8-yl)-2-ureidobutanamide		
30		19.53 ± 2.83	23%
	N-(4-methoxybenzyl)-5,7-dimethyl-[1,2,4]triazolo[1,5-a]pyrimidine-2-carboxamide		
31		30%	37%
	8-hydrazinyl-7-(2-hydroxy-3-isopropoxypropyl)-3-methyl-1H-purine-2,6(3H,7H)-dione		
32		32%	34%
	1-allyl-2-hydroxy-4-oxo-N-phenethyl-1,4-dihydroquinoline-3-carboxamide		
33		17%	42%
	2-(3-(3-acetylphenyl)ureido)benzamide		
34		14%	48.13 ± 4.34
	(E)-3-(2-chloro-6-fluorophenyl)-N-(1-phenylethyl)acrylamide		
MG-132		0.13 ± 0.01	0.072 ± 0.014

The thirty-four identified hits are characterized by a central amide moiety except for compounds **17** and **31** which are, respectively, a purine derivative and a carboxylate derivative. Compounds **15**, **25**, and **35** have a central urea moiety. All the hits showed aromatic substituents on both sides of the amide moiety except for compounds **5**, **7**, **10**, **27**, and **29**, which have just aromatic substituents at one side of the central core. Compounds bearing pyrrole, pyrazole, and/or imidazole moieties showed no inhibition or low inhibition on $\beta 1i$ and $\beta 5i$ subunits, respectively.

As shown in Table 1, some of the tested compounds were active on the immunoproteasome, with K_i values in the micromolar range (**2**, **3**, **13**, **14**, **17**, **30**, and **34**). Interestingly, as observed in the in silico studies, compound **2** inhibits both subunits ($K_i = 12.53 \pm 0.18 \mu\text{M}$ for $\beta 1i$ and $31.95 \pm 0.81 \mu\text{M}$ for $\beta 5i$). In Figure 7, the binding modes of compound **2**, obtained by IFD, are reported. The central amide moiety establishes an H-bond with the key residue Thr13 in both subunits. The furane ring forms a π -stacking interaction with Phe31 and Tyr169 in $\beta 1i$ and $\beta 5i$ subunits, respectively. An additional H-bond is established with Thr21 and the quinolinone moiety in $\beta 5i$.

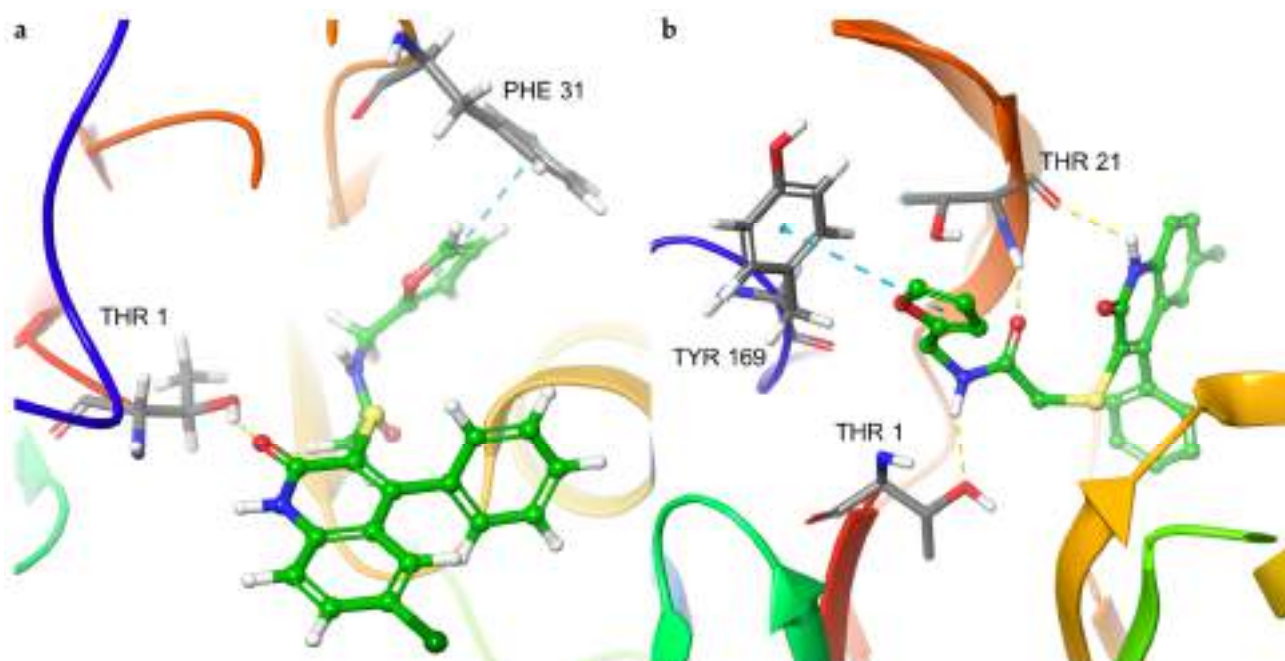
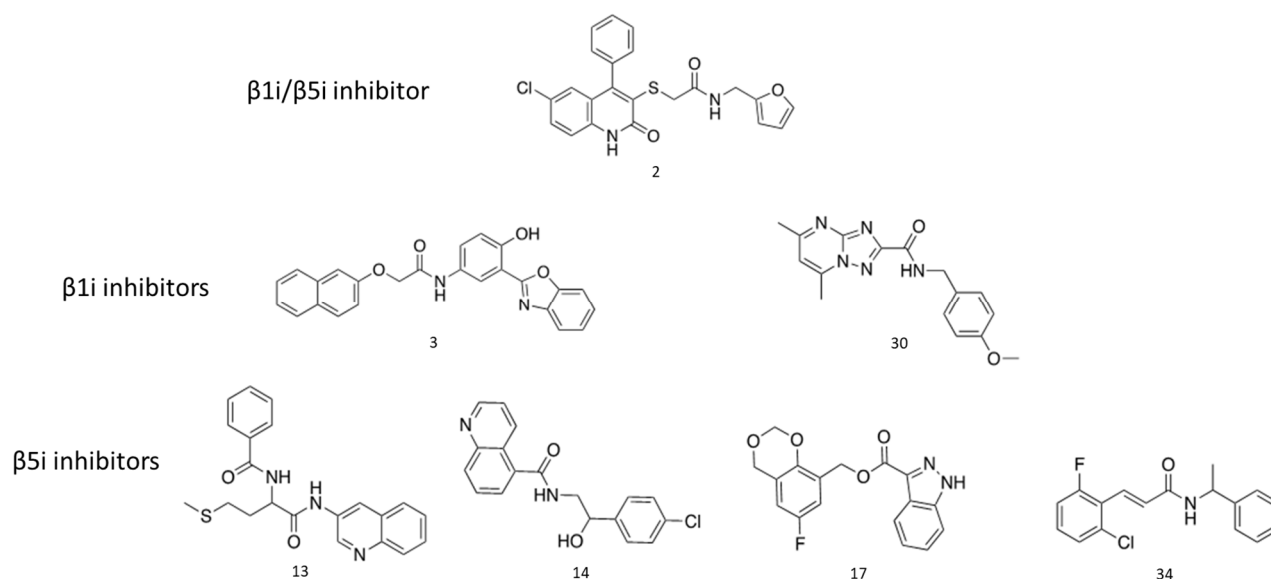


Figure 7. Binding mode of **2** into the active site of (a) $\beta 1i$ and (b) $\beta 5i$ subunits. The H-bonds are represented in yellow dashes and the π -stacking in blue dashes.

Compounds **3** and **30** inhibit $\beta 1i$ subunits. Structurally, compound **3** shows an isosteric substitution of an oxygen atom in place of a sulfur atom and a naphthyl ring in place of a quinolinone moiety. This moiety is replaced by a triazolopyrimidine in compound **30**, which is bound to the amide moiety without the thioether or ether chain as in the previous inhibitor. Compounds **13**, **14**, **17**, and **34** inhibit $\beta 5i$. Interestingly, compound **17** is the only inhibitor that does not bear an amide moiety in the central core.

These newly identified hits could be interesting for further optimization. The amide moiety remains a key pharmacophore that is surrounded by the right combination of aromatic moieties and could lead to more active non-peptide and non-covalent inhibitors (Scheme 2).



Scheme 2. Most active compounds retrieved.

3. Materials and Methods

3.1. System and Ligand Preparations

For this study, we selected the amino acid chain K from the 20S mouse immunoproteasome crystallographic structure at 2.90 Å resolution (PDB ID: 3UNF) [30], corresponding to the $\beta 5i$ subunit with the co-crystallized ligand PR-957.

As reported in the previous paper, the reactive residue at the catalytic site, in this case, Thr1, was reconstituted after the removal of the covalent inhibitor by breaking the covalent bond and filling the open valence. Then, the structure and PR-957 were refined and optimized using the Protein Preparation Wizard (Schrödinger New York, 2021-1) and LigPrep (Schrödinger New York, 2021-1). OPLS2005 [31] was used as the force field and Epik (Schrödinger New York, 2021-1) was selected as the ionization tool at $\text{pH } 7.2 \pm 0.2$.

A validation dataset containing active and decoy compounds was prepared for virtual screening. Active compounds on $\beta 1$ and $\beta 5$ subunits were obtained from the literature [23,32–35] for both subunits, while decoys were obtained from the DUD-E database [36] and filtered to remove duplicates. For each active compound in the dataset, 50 decoys were generated. An in-house and two commercial libraries (Asinex and Bioscient) containing >300,000 compounds were prepared in SDF format. The libraries were pre-filtered to remove groups classified as Tox-Alerts, Pan Assays INterference compounds (PAINS), and Rapid Elimination Of Swills (REOS), which can give false positives due to non-specific reactions during testing [37,38]. As for PR-957, validation, in-house, and commercial libraries were prepared and optimized using LigPrep.

3.2. Pharmacophore Modeling Generation

LigandScout and PHASE (Schrödinger, LLC, New York, NY, USA, 2021) were used to generate dynamic pharmacophore models for $\beta 1i$ and structure-based pharmacophore model based on the experimental structure of the $\beta 5i$ subunit.

The models were generated using the following merged pharmacophore creation settings: Feature tolerance scale factor = 1.0; Maximum number of resulting pharmacophores = 10; Number of omitted features for merged pharmacophore = 4.

The structure-based pharmacophore model for the $\beta 5i$ subunit was generated, starting from the PDB coordinate set of $\beta 5i$ subunit-PR-957. The resulting models were validated for their performance in discriminating between the active and decoy molecules using specific databases for $\beta 1i$ and $\beta 5i$.

A consensus score was calculated. It combined the normalized scores obtained from the Pharmacophore-Fit Score from LigandScout and the Phase-Fit Score from Phase, as shown in Equation (1).

$$\text{Consensus} = \left(\frac{\text{Pharmacophore Fit Score}}{10} + \frac{\text{Phase Score}}{3} \right) \quad (1)$$

3.3. Molecular Docking

The docking study was performed using the Glide docking tool v. 9.0. [39].

The grid box was set on the PR-957 ligand coordinates. The Van der Waals radius was 1 Å, and the partial charge cut-off was 0.15 Å with flexible ligand sampling. Bias sampling torsion penalization for amides with non-planar conformation and Epik state penalties were added to the docking score. To validate the docking protocol and evaluate the ability to reproduce the experimental pose of the co-crystallized ligand, the re-docking test was performed with XP-level precision. The validation of the docking is carried out through the calculation of the RMSD of the cognate ligand, which gives an indication of the deviation between the experimental pose of the ligand and that reproduced by the docking algorithm. The reference value for RMSD is <2.0 for the scoring function.

The Virtual Screening was performed in three different docking steps: High Throughput Virtual Screening (HTVS), Standard Precision (SP), and Extra Precision (XP). Each docking step was run unconstrained.

3.4. Induced Fit Docking (IFD)

Induced Fit Docking (IFD) developed by Schrödinger [40] was performed using the standard protocol, as reported in the different studies [24,29,41–45]. The receptor box for β5i was set on the PR-957 pose with no constraints applied. The receptor box for β1i was defined on the residues Ser21, Phe31, Ser33, and Gly47.

3.5. In Vitro 20S Immunoproteasome Inhibition Assays

Human 20S immunoproteasome, obtained from the human spleen, was purchased from Enzo Life Science. The hydrolysis of the appropriate peptidyl 7-amino-4-methyl coumarin (AMC) substrate was monitored to measure the proteolytic activities of the immunoproteasome. The substrates Suc-Leu-Leu-Val-Tyr-AMC (Bachem, Bubendorf, Switzerland) for β5i and Ac-Pro-Ala-Leu-AMC (Biomol GmbH, Hamburg, Germany) for β1i subunits were used at 50 μM. Fluorescence of the hydrolysis product AMC was measured at 30 °C with a 380 nm excitation filter and a 460 nm emission filter using an Infinite 200 PRO microplate reader (Tecan, Männedorf, Switzerland). A preliminary screening at 100 μM inhibitor concentrations was carried out on the two proteolytic activities of the immunoproteasome.

An equivalent amount of DMSO as a negative control and compound 1 and MG-132 (a reversible immunoproteasome inhibitor) as a positive control were used for β1i and β5i, respectively. Compounds showing at least 50% inhibition at the screening concentration were then progressed into detailed assays. Continuous assays were performed at seven different concentrations ranging from 100 μM to 5 μM and by calculating the dissociation constants K_i of the enzyme–inhibitor complex using the Cheng–Prusoff equation, $K_i = \text{IC}_{50} / (1 + [\text{S}]K_m^{-1})$. Inhibitor solutions were prepared from stocks in DMSO. Each independent assay was duplicated in 96-well plates with a total volume of 200 μL. For the assay on β1i and β5i subunits, a human 20S immunoproteasome was incubated at 30 °C at a final concentration of 4 μg/mL with the inhibitor at seven different concentrations. The reaction buffer comprised Tris·HCl (50 mM, pH 7.4), KCl (25 mM), NaCl (10 mM), MgCl₂ (1 mM), and 0.03% SDS. AMC released from substrate hydrolysis was monitored in a kinetic cycle for 10 min.

4. Conclusions

In this work, we report a virtual screening strategy built on a dynamic pharmacophore modeling approach onto the β 1i subunit and a pharmacophore/docking approach onto the β 5i subunit of the immunoproteasome. The outcomes of the computational approaches led to the identification of thirty-four hit compounds selected from three libraries. These hit compounds were tested in in vitro enzymatic assays and seven (**2**, **3**, **13**, **15**, **17**, **30**, and **34**) were active on the immunoproteasome, with K_i values in the micromolar range. Compound **3** and compound **17** are the most active against the β 1i subunit and β 5i subunit, respectively. Interestingly, Compound **2** showed inhibitory activity on both subunits, and induced fit docking analysis revealed a binding pattern onto β 1i with Thr1 and Phe31 that represent new key residues as reported in our previous work. Onto β 5i subunit, it interacts with the key residues Thr1, Thr21, and Tyr169. The hit compounds identified represent an interesting starting point for further optimization. Compound **2** showed a dual inhibition and some key pharmacophoric features that could be exploited to identify more potent inhibitors. Moreover, we are planning to investigate the anti-inflammatory profile of β 5i-inhibitors and the anticancer activity of β 1i-inhibitors, since an up-regulation of the corresponding β i subunits has been detected in inflammatory diseases or hematological malignancies, respectively, in future studies.

Author Contributions: Conceptualization, M.Z., G.C. and M.T.; methodology, M.T., G.C. and U.P.; software, G.C.; validation, M.T., G.C. and U.P.; formal analysis, R.E. and C.D.C.; data curation, M.T., G.C., U.P., R.E. and C.D.C.; writing—original draft preparation, all the authors; writing—review and editing, all the authors; supervision, A.M.A., M.Z.; project administration, M.Z.; funding acquisition, M.Z. All authors have read and agreed to the published version of the manuscript.

Funding: FFR-D15-161363 University of Palermo.

Data Availability Statement: The authors will provide the data if requested.

Conflicts of Interest: The authors declare no conflict of interest.

References

1. Micale, N.; Scarbaci, K.; Troiano, V.; Ettari, R.; Grasso, S.; Zappalà, M. Peptide-Based Proteasome Inhibitors in Anticancer Drug Design. *Med. Res. Rev.* **2014**, *34*, 1001–1069. [[CrossRef](#)] [[PubMed](#)]
2. DeMartino, G.N.; Gillette, T.G. Proteasomes: Machines for All Reasons. *Cell* **2007**, *129*, 659–662. [[CrossRef](#)] [[PubMed](#)]
3. Weissman, A.M.; Shabek, N.; Ciechanover, A. The Predator Becomes the Prey: Regulating the Ubiquitin System by Ubiquitylation and Degradation. *Nat. Rev. Mol. Cell Biol.* **2011**, *12*, 605–620. [[CrossRef](#)] [[PubMed](#)]
4. Ciechanover, A.; Schwartz, A.L. The Ubiquitin System: Pathogenesis of Human Diseases and Drug Targeting. *Biochim. Biophys. Acta Mol. Cell Res.* **2004**, *1695*, 3–17. [[CrossRef](#)]
5. Kisselev, A.F.; Van Der Linden, W.A.; Overkleeft, H.S. Proteasome Inhibitors: An Expanding Army Attacking a Unique Target. *Chem. Biol.* **2012**, *19*, 99–115. [[CrossRef](#)]
6. Sahu, I.; Mali, S.M.; Sulkshane, P.; Xu, C.; Rozenberg, A.; Morag, R.; Sahoo, M.P.; Singh, S.K.; Ding, Z.; Wang, Y.; et al. The 20S as a Stand-Alone Proteasome in Cells Can Degrade the Ubiquitin Tag. *Nat. Commun.* **2021**, *12*, 6173. [[CrossRef](#)]
7. Kisselev, A.F.; Callard, A.; Goldberg, A.L. Importance of the Different Proteolytic Sites of the Proteasome and the Efficacy of Inhibitors Varies with the Protein Substrate. *J. Biol. Chem.* **2006**, *281*, 8582–8590. [[CrossRef](#)]
8. Ettari, R.; Previti, S.; Bitto, A.; Grasso, S.; Zappalà, M. Immunoproteasome-Selective Inhibitors: A Promising Strategy to Treat Hematologic Malignancies, Autoimmune and Inflammatory Diseases. *Curr. Med. Chem.* **2016**, *23*, 1217–1238. [[CrossRef](#)]
9. Ettari, R.; Zappalà, M.; Grasso, S.; Musolino, C.; Innao, V.; Allegra, A. Immunoproteasome-Selective and Non-Selective Inhibitors: A Promising Approach for the Treatment of Multiple Myeloma. *Pharmacol. Ther.* **2018**, *182*, 176–192. [[CrossRef](#)]
10. De Bruin, G.; Huber, E.M.; Xin, B.T.; Van Rooden, E.J.; Al-Ayed, K.; Kim, K.B.; Kisselev, A.F.; Driessen, C.; Van Der Stelt, M.; Van Der Marel, G.A.; et al. Structure-Based Design of B1i or B5i Specific Inhibitors of Human Immunoproteasomes. *J. Med. Chem.* **2014**, *57*, 6197–6209. [[CrossRef](#)]
11. Johnson, H.W.B.; Anderl, J.L.; Bradley, E.K.; Bui, J.; Jones, J.; Arastu-Kapur, S.; Kelly, L.M.; Lowe, E.; Moebius, D.C.; Muchamuel, T.; et al. Discovery of Highly Selective Inhibitors of the Immunoproteasome Low Molecular Mass Polypeptide 2 (LMP2) Subunit. *ACS Med. Chem. Lett.* **2017**, *8*, 413–417. [[CrossRef](#)] [[PubMed](#)]

12. Johnson, H.W.B.; Lowe, E.; Anderl, J.L.; Fan, A.; Muchamuel, T.; Bowers, S.; Moebius, D.C.; Kirk, C.; McMinn, D.L. Required Immunoproteasome Subunit Inhibition Profile for Anti-Inflammatory Efficacy and Clinical Candidate KZR-616 ((2S,3R)-N-((S)-3-(Cyclopent-1-En-1-Yl)-1-((R)-2-Methyloxiran-2-Yl)-1-Oxopropan-2-Yl)-3-Hydroxy-3-(4-Methoxyphenyl)-2-((S)-2-(2-Morpholinoacetamido)Propanamido)Propenamido)Propenamido). *J. Med. Chem.* **2018**, *61*, 11127–11143. [[CrossRef](#)] [[PubMed](#)]
13. Kaiser, M.; Groll, M.; Siciliano, C.; Assfalg-Machleidt, I.; Weyher, E.; Kohno, J.; Milbradt, A.G.; Renner, C.; Huber, R.; Moroder, L. Binding Mode of TMC-95A Analogues to Eukaryotic 20S Proteasome. *ChemBioChem* **2004**, *5*, 1256–1266. [[CrossRef](#)] [[PubMed](#)]
14. Groll, M.; Gallastegui, N.; Maréchal, X.; Le Ravalec, V.; Basse, N.; Richy, N.; Genin, E.; Huber, R.; Moroder, L.; Vidal, J.; et al. 20S Proteasome Inhibition: Designing Noncovalent Linear Peptide Mimics of the Natural Product TMC-95A. *ChemMedChem* **2010**, *5*, 1701–1705. [[CrossRef](#)] [[PubMed](#)]
15. Gallastegui, N.; Beck, P.; Arciniega, M.; Huber, R.; Hillebrand, S.; Groll, M. Hydroxyureas as Noncovalent Proteasome Inhibitors. *Angew. Chem.-Int. Ed.* **2012**, *51*, 247–249. [[CrossRef](#)] [[PubMed](#)]
16. Santos, R.D.L.A.; Bai, L.; Singh, P.K.; Murakami, N.; Fan, H.; Zhan, W.; Zhu, Y.; Jiang, X.; Zhang, K.; Assker, J.P.; et al. Structure of Human Immunoproteasome with a Reversible and Noncompetitive Inhibitor That Selectively Inhibits Activated Lymphocytes. *Nat. Commun.* **2017**, *8*, 1692. [[CrossRef](#)]
17. Ettari, R.; Bonaccorso, C.; Micale, N.; Heindl, C.; Schirmeister, T.; Calabrò, M.L.; Grasso, S.; Zappalà, M. Development of Novel Peptidomimetics Containing a Vinyl Sulfone Moiety as Proteasome Inhibitors. *ChemMedChem* **2011**, *6*, 1228–1237. [[CrossRef](#)]
18. Micale, N.; Ettari, R.; Lavecchia, A.; Di Giovanni, C.; Scarbaci, K.; Troiano, V.; Grasso, S.; Novellino, E.; Schirmeister, T.; Zappalà, M. Development of Peptidomimetic Boronates as Proteasome Inhibitors. *Eur. J. Med. Chem.* **2013**, *64*, 23–34. [[CrossRef](#)]
19. Scarbaci, K.; Troiano, V.; Micale, N.; Ettari, R.; Tamborini, L.; Di Giovanni, C.; Cerchia, C.; Grasso, S.; Novellino, E.; Schirmeister, T.; et al. Identification of a New Series of Amides as Non-Covalent Proteasome Inhibitors. *Eur. J. Med. Chem.* **2014**, *76*, 1–9. [[CrossRef](#)]
20. Troiano, V.; Scarbaci, K.; Ettari, R.; Micale, N.; Cerchia, C.; Pinto, A.; Schirmeister, T.; Novellino, E.; Grasso, S.; Lavecchia, A.; et al. Optimization of Peptidomimetic Boronates Bearing a P3 Bicyclic Scaffold as Proteasome Inhibitors. *Eur. J. Med. Chem.* **2014**, *83*, 1–14. [[CrossRef](#)]
21. Scarbaci, K.; Troiano, V.; Ettari, R.; Pinto, A.; Micale, N.; Di Giovanni, C.; Cerchia, C.; Schirmeister, T.; Novellino, E.; Lavecchia, A.; et al. Development of Novel Selective Peptidomimetics Containing a Boronic Acid Moiety, Targeting the 20S Proteasome as Anticancer Agents. *ChemMedChem* **2014**, *9*, 1801–1816. [[CrossRef](#)] [[PubMed](#)]
22. Di Giovanni, C.; Ettari, R.; Sarno, S.; Rotondo, A.; Bitto, A.; Squadrito, F.; Altavilla, D.; Schirmeister, T.; Novellino, E.; Grasso, S.; et al. Identification of Noncovalent Proteasome Inhibitors with High Selectivity for Chymotrypsin-like Activity by a Multistep Structure-Based Virtual Screening. *Eur. J. Med. Chem.* **2016**, *121*, 578–591. [[CrossRef](#)] [[PubMed](#)]
23. Ettari, R.; Cerchia, C.; Maiorana, S.; Guccione, M.; Novellino, E.; Bitto, A.; Grasso, S.; Lavecchia, A.; Zappalà, M. Development of Novel Amides as Noncovalent Inhibitors of Immunoproteasomes. *ChemMedChem* **2019**, *14*, 842–852. [[CrossRef](#)] [[PubMed](#)]
24. Culetta, G.; Zappalà, M.; Ettari, R.; Almerico, A.M.; Tutone, M. Immunoproteasome and Non-Covalent Inhibition: Exploration by Advanced Molecular Dynamics and Docking Methods. *Molecules* **2021**, *26*, 4046. [[CrossRef](#)] [[PubMed](#)]
25. Wolber, G.; Langer, T. LigandScout: 3-D Pharmacophores Derived from Protein-Bound Ligands and Their Use as Virtual Screening Filters. *J. Chem. Inf. Model.* **2005**, *45*, 160–169. [[CrossRef](#)]
26. Dixon, S.L.; Smondyrev, A.M.; Rao, S.N. PHASE: A Novel Approach to Pharmacophore Modeling and 3D Database Searching. *Chem. Biol. Drug Des.* **2006**, *67*, 370–372. [[CrossRef](#)]
27. Perricone, U.; Wieder, M.; Seidel, T.; Langer, T.; Padova, A.; Almerico, A.M.; Tutone, M. A Molecular Dynamics-Shared Pharmacophore Approach to Boost Early-Enrichment Virtual Screening: A Case Study on Peroxisome Proliferator-Activated Receptor α . *ChemMedChem* **2017**, *12*, 1399–1407. [[CrossRef](#)]
28. Culetta, G.; Allegra, M.; Almerico, A.M.; Restivo, I.; Tutone, M. In Silico Design, Synthesis and Biological Evaluation of Anticancer Arylsulfonamide Endowed with Anti-Telomerase Activity. *Pharmaceuticals* **2022**, *15*, 82. [[CrossRef](#)]
29. Culetta, G.; Gulotta, M.R.; Perricone, U.; Zappalà, M.; Almerico, A.M.; Tutone, M. Exploring the SARS-CoV-2 Proteome in the Search of Potential Inhibitors via Structure-Based Pharmacophore Modeling/Docking Approach. *Computation* **2020**, *8*, 77. [[CrossRef](#)]
30. Huber, E.M.; Basler, M.; Schwab, R.; Heinemeyer, W.; Kirk, C.J.; Groettrup, M.; Groll, M. Immuno- and Constitutive Proteasome Crystal Structures Reveal Differences in Substrate and Inhibitor Specificity. *Cell* **2012**, *148*, 727–738. [[CrossRef](#)]
31. Robertson, M.J.; Tirado-Rives, J.; Jorgensen, W.L. Improved Peptide and Protein Torsional Energetics with the OPLS-AA Force Field. *J. Chem. Theory Comput.* **2015**, *11*, 3499–3509. [[CrossRef](#)] [[PubMed](#)]
32. Ettari, R.; Iraci, N.; Di Chio, C.; Previti, S.; Danzè, M.; Zappalà, M. Development of Isoquinolinone Derivatives as Immunoproteasome Inhibitors. *Bioorg. Med. Chem. Lett.* **2022**, *55*, 128478. [[CrossRef](#)] [[PubMed](#)]
33. Villoutreix, B.O.; Khatib, A.M.; Cheng, Y.; Miteva, M.A.; Maréchal, X.; Vidal, J.; Reboud-Ravaux, M. Blockade of the Malignant Phenotype by β -Subunit Selective Noncovalent Inhibition of Immuno- and Constitutive Proteasomes. *Oncotarget* **2017**, *8*, 10437–10449. [[CrossRef](#)] [[PubMed](#)]
34. Zhan, W.; Singh, P.K.; Ban, Y.; Qing, X.; Ah Kioon, M.D.; Fan, H.; Zhao, Q.; Wang, R.; Sukenick, G.; Salmon, J.; et al. Structure-Activity Relationships of Noncovalent Immunoproteasome B5i-Selective Dipeptides. *J. Med. Chem.* **2020**, *63*, 13103–13123. [[CrossRef](#)] [[PubMed](#)]

35. Ettari, R.; Pallio, G.; Pizzino, G.; Irrera, N.; Zappalà, M.; Maiorana, S.; Di Chio, C.; Altavilla, D.; Squadrito, F.; Bitto, A. Non-Covalent Immunoproteasome Inhibitors Induce Cell Cycle Arrest in Multiple Myeloma MM.1R Cells. *J. Enzyme Inhib. Med. Chem.* **2019**, *34*, 1307–1313. [[CrossRef](#)] [[PubMed](#)]
36. Mysinger, M.M.; Carchia, M.; Irwin, J.J.; Shoichet, B.K. Directory of Useful Decoys, Enhanced (DUD-E): Better Ligands and Decoys for Better Benchmarking. *J. Med. Chem.* **2012**, *55*, 6582–6594. [[CrossRef](#)] [[PubMed](#)]
37. Lipinski, C.A. Lead- and Drug-like Compounds: The Rule-of-Five Revolution. *Drug Discov. Today Technol.* **2004**, *1*, 337–341. [[CrossRef](#)]
38. Baell, J.B.; Nissink, J.W.M. Seven Year Itch: Pan-Assay Interference Compounds (PAINS) in 2017—Utility and Limitations. *ACS Chem. Biol.* **2018**, *13*, 36–44. [[CrossRef](#)]
39. Friesner, R.A.; Murphy, R.B.; Repasky, M.P.; Frye, L.L.; Greenwood, J.R.; Halgren, T.A.; Sanschagrin, P.C.; Mainz, D.T. Extra Precision Glide: Docking and Scoring Incorporating a Model of Hydrophobic Enclosure for Protein-Ligand Complexes. *J. Med. Chem.* **2006**, *49*, 6177–6196. [[CrossRef](#)]
40. Sherman, W.; Day, T.; Jacobson, M.P.; Friesner, R.A.; Farid, R. Novel Procedure for Modeling Ligand/Receptor Induced Fit Effects. *J. Med. Chem.* **2006**, *49*, 534–553. [[CrossRef](#)]
41. Allegra, M.; Tutone, M.; Tesoriere, L.; Attanzio, A.; Culetta, G.; Almerico, A.M. Evaluation of the IKK β Binding of Indicaxanthin by Induced-Fit Docking, Binding Pose Metadynamics, and Molecular Dynamics. *Front. Pharmacol.* **2021**, *12*, 701568. [[CrossRef](#)] [[PubMed](#)]
42. Tutone, M.; Pibiri, I.; Lentini, L.; Pace, A.; Almerico, A.M. Deciphering the Nonsense Readthrough Mechanism of Action of Ataluren: An in Silico Compared Study. *ACS Med. Chem. Lett.* **2019**, *10*, 522–527. [[CrossRef](#)] [[PubMed](#)]
43. Tutone, M.; Virzì, A.; Almerico, A.M. Reverse Screening on Indicaxanthin from *Opuntia Ficus-Indica* as Natural Chemoactive and Chemopreventive Agent. *J. Theor. Biol.* **2018**, *455*, 147–160. [[CrossRef](#)] [[PubMed](#)]
44. Tutone, M.; Chinnici, A.; Almerico, A.M.; Perricone, U.; Sutura, F.M.; De Caro, V. Design, Synthesis and Preliminary Evaluation of Dopamine-Amino Acid Conjugates as Potential D1 Dopaminergic Modulators. *Eur. J. Med. Chem.* **2016**, *124*, 435–444. [[CrossRef](#)] [[PubMed](#)]
45. Allegra, M.; Tutone, M.; Tesoriere, L.; Almerico, A.M.; Culetta, G.; Livrea, M.A.; Attanzio, A. Indicaxanthin, a multi-target natural compound from *Opuntia ficus-indica* fruit: From its poly-pharmacological effects to biochemical mechanisms and molecular modelling studies. *Eur. J. Med. Chem.* **2019**, *179*, 753–764. [[CrossRef](#)] [[PubMed](#)]

Disclaimer/Publisher’s Note: The statements, opinions and data contained in all publications are solely those of the individual author(s) and contributor(s) and not of MDPI and/or the editor(s). MDPI and/or the editor(s) disclaim responsibility for any injury to people or property resulting from any ideas, methods, instructions or products referred to in the content.